Association of Vascular ^{18}F-FDG Uptake with Vascular Calcification

Mark P.S. Dunphy, DO[1]; Alvin Freiman, MD[2]; Steven M. Larson, MD[1]; and H. William Strauss, MD[1]

[1]*Nuclear Medicine Service, Department of Radiology, Memorial Sloan-Kettering Cancer Center, New York, New York; and*
[2]*Department of Cardiology, Memorial Sloan-Kettering Cancer Center, New York, New York*

Both calcification and FDG uptake have been advocated as indicators of atheroma. Atheromas calcify as cells in the lesion undergo apoptosis and necrosis during evolution of the lesion and at the end stage of the lesion. FDG concentrates in lesions due to the relatively dense cellularity in regions of inflammation of active atheromas. This investigation examines the geographic relationship of focal vascular ^{18}F-FDG uptake, as a marker of atherosclerotic inflammation, to arterial calcification detected by contemporaneous CT. **Methods:** We reviewed PET/CT images from 78 patients who were referred for tumor staging for the presence of vascular ^{18}F-FDG uptake and vascular calcification. Arterial wall ^{18}F-FDG accumulation greater than adjacent blood-pool activity was considered inflammation. Arterial attenuation of >130 Hounsfield units was considered calcification. Sites in the ascending and descending aorta, the carotid and iliac arteries, and the coronary territories were examined on the emission, CT, and fusion images on a point-by-point basis. When lesions were seen, we evaluated whether they were overlapping or discrete. **Results:** The ^{18}F-FDG arterial distribution was consistent with established atherosclerotic topography, with increased uptake in the thoracic aorta, at the carotid bifurcation, and in the proximal coronary vessels. Arteries typically displayed a patchwork of normal vessel, focal inflammation, or calcification; inflammation and calcification overlapped in <2% of cases. Arterial inflammation preceded calcification, in terms of mean patient age. Coronary inflammation was more prevalent in patients with more cardiovascular risk factors. **Conclusion:** Vascular calcification and vascular metabolic activity rarely overlap, suggesting these findings represent different stages in the evolution of atheroma.

Key Words: atherosclerosis; tomography; calcium; imaging; inflammation

J Nucl Med 2005; 46:1278–1284

Atherosclerosis is an immune inflammatory disease (*1*) characterized by subendothelial lipid accumulation, monocyte/macrophage accrual (*2*), and vascular calcification (*3*). Using the glucose analog ^{18}F-FDG, PET can image vascular inflammation (*4–6*), primarily due to increased macrophage metabolism (*7–9*). Rudd et al. identified increased ^{18}F-FDG uptake in carotid plaques in a small group of patients before cartotid endarterectomy (*10*). Histopathology of the lesions demonstrated more macrophages in ^{18}F-FDG–positive lesions, whereas calcium and fibrous tissue were more prevalent in the ^{18}F-FDG–negative lesions. ^{18}F-FDG accumulation in the arterial tree of cancer patients who were referred for PET occurs relatively frequently (*11,12*). Similarly, arterial calcification, another marker of atheroma (*13,14*), is often observed in the CT studies performed on these patients. This investigation compares the regional distribution of arterial ^{18}F-FDG uptake and calcification on a point-by-point basis in the arterial tree of a series of patients who were referred for PET/CT in the course of tumor staging.

MATERIALS AND METHODS

Patients

PET/CT data of 78 consecutive patients (51 men, 27 women; median age, 67 y; age range, 10–86 y) who were referred for tumor staging were reviewed. The study protocol was approved by the Memorial Sloan-Kettering Cancer Center institutional review board. The patient's age, medications, and blood sugar at the time of injection were recorded.

PET/CT and Image Reconstruction

PET/CT images were recorded with a Biograph (Siemens/CTI) or Discovery (GE Healthcare) system. Data were recorded from the level of the auditory meatus to the midthigh 72 ± 18 min (mean ± SD) after intravenous injection of 475 ± 59 MBq (mean ± SD) ^{18}F-FDG. Activity was scaled to body surface area for pediatric patients (n = 3). After a scout view, noncontrast spiral CT was performed at 50 mA and 130 kVp (Siemens/CTI) or 80 mA and 140 kVp (GE Healthcare). Emission data were then obtained for 3 min per bed position with each instrument (3-dimensional on the Biograph and 2-dimensional on the Discovery).

Image Analysis

CT images were evaluated for calcification in the carotid, coronary, aortic, and iliac arteries (vascular attenuation of >130 Hounsfield units) (*15*). To detect overlap of ^{18}F-FDG and calcification, the PET/CT fusion images were used. In addition, the fusion data were also used for anatomic localization of focal ^{18}F-FDG uptake. Attenuation-corrected and uncorrected PET images were evaluated. Regions of interest (ROIs) were drawn at the bifurcation of the pulmonary artery; left atrium; and 3 aortic regions (level with the tracheal bifurcation, diaphragmatic crura,

Received Feb. 9, 2005; revision accepted Apr. 5, 2005.
For correspondence or reprints contact: Mark P.S. Dunphy, DO, Nuclear Medicine Service, Department of Radiology, Memorial Sloan-Kettering Cancer Center, Room S-212, New York, New York, 10021.
E-mail: dunphym@mskcc.org

and proximal to the aortic bifurcation). Mean blood-pool activity was calculated. The lower threshold of the PET color scale was raised to exclude blood-pool activity (Fig. 1).

^{18}F-FDG activity that followed arterial contours on the fused CT image, in 3 orthogonal views, was considered as possible inflammation. For the coronary arteries, arterial wall activity was defined as ^{18}F-FDG accumulation within the expected anatomic distribution of the coronary arteries in 3 orthogonal views, allowing for cardiac motion artifact (*16*). When intense myocardial uptake was present (defined as visualization of epi- or endocardial borders of any myocardial segment), coronary vessels were excluded from analysis. After analyzing PET/CT images, medical records were reviewed to determine cardiac risk factors and identify patients with subsequent cardiovascular events.

Myocardial Perfusion Imaging (MPI)

Thirty-two patients also had SPECT gated MPI within 1 mo of PET/CT. MPI was performed by a rest–stress protocol, injecting 370 and 925 MBq ^{99m}Tc-tetrofosmin (n = 10) or a combination (n = 22) of 148 MBq ^{201}Tl chloride at rest and 925 MBq ^{99m}Tc-tetrofosmin at stress. Stress was induced by Bruce treadmill exercise (n = 12) or adenosine infusion (n = 20). Gated SPECT images were acquired as soon as possible after stress. Perfusion status (i.e., normal, ischemia, infarct) was taken from the original MPI reports.

Statistics

Site-specific blood-pool activities were compared using between-subjects ANOVA. The proportion of cases showing arterial ^{18}F-FDG uptake in each territory was analyzed by confidence intervals (CIs) (modified Wald method) and ANOVA. Using odds ratios (ORs) with CIs, we compared territorial ^{18}F-FDG uptake with calcification and coronary ^{18}F-FDG uptake with (a) history of coronary artery disease (CAD), (b) cardiac risk factors (i.e., hypertension, diabetes, hypercholesterolemia, smoking history, and age >45 y for men and >55 y for women), and (c) MPI. Significance was assessed by the Fisher exact test. Similarly, we compared carotid ^{18}F-FDG uptake and cardiac risk factors. Two-tailed P values of 0.05 were taken as significant, with correction for multiple comparisons.

RESULTS

A summary of the patients' age and risk factors is presented in Table 1. All patients were euglycemic at the time of ^{18}F-FDG injection. Malignancies were found in 73 patients: 3 breast, 9 endocrine, 28 gastrointestinal, 4 genitourinary, 11 hematologic, 2 musculoskeletal, and 16 respiratory cancers; 5 patients had no cancer. Three patients were treated with potent antiinflammatory agents at the time of ^{18}F-FDG injection: one each with dexamethasone, tacrolimus, and prednisone. All had significant ^{18}F-FDG uptake in their major vessels.

Blood-Pool Activity

Mean blood-pool activities in the 5 arterial ROIs were not significantly different (P = 0.5), with an average coefficient of variation of 13.5%, most likely due to differences in vessel size at each measured location.

Arterial ^{18}F-FDG Uptake and Calcification

Vessels demonstrated a patchwork of ^{18}F-FDG uptake, calcification, and normal vessel (neither ^{18}F-FDG nor calcium). Arterial ^{18}F-FDG uptake and calcification were common in all examined territories but rarely overlapped (<2% of vascular territories). Table 2 lists the results in the 82 studies performed on 78 patients (4 patients had prior PET scans that are included in the analysis). Calcification was associated with significantly greater odds of adjacent local vascular ^{18}F-FDG uptake, particularly in the abdominal aorta (Table 3).

^{18}F-FDG accumulation was seen in the aortae of 61 patients (74%), 21 (45%) sets of coronary arteries, and 26 (31%) carotid and 28 (34%) iliac pairs (Fig. 2). Aortic ^{18}F-FDG uptake was most commonly proximal (52%), followed by abdominal (48%), and descending thoracic (31%) segments. Calcification was more common than ^{18}F-FDG uptake in all arterial regions, except the carotids (31% vs. 19% of patients, respectively) and proximal aorta (52% vs. 46%, respectively).

Patients with arterial ^{18}F-FDG accumulation were younger, on average, than patients with arterial calcification, in most territories. No patient had a history of vasculitis.

Seven patients had abdominal aortic aneurysms (AAA). Three AAA were ^{18}F-FDG avid (Fig. 3). ^{18}F-FDG–positive

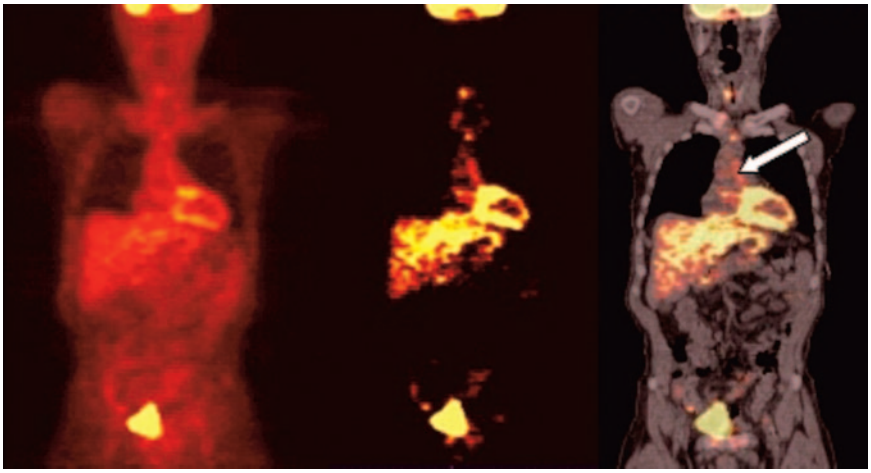

FIGURE 1. (Left) Coronal ^{18}F-FDG PET image of upper body. (Center) Intensity adjustment based on blood-pool activity. (Right) CT fused with adjusted PET image shows inflammation in wall of ascending aorta (arrow).

TABLE 1
Study Population Characteristics

Sex	n*	Age (y) (mean)	No. of risk factors†					
			0	1	2	3	4	5
Male	51	10–86 (70)	2	10	17	14	6	2
Female	27	17–76 (59)	9	7	4	4	2	1
Total	78	10–86 (67)	11	17	21	18	8	3

*Sample size.
†Risk factors: hypertension, diabetes, smoking history, hypercholesterolemia, age (>45 y for men and >55 y for women).

aneurysms measured 3.0, 5.3, and 5.6 cm in greatest transaxial diameter on CT. The 4 AAA without ^{18}F-FDG uptake were ≤3.4 cm. The patient with the largest AAA had chronic abdominal pain at the time of PET. Three patients had prior surgical repair: the patient with the largest AAA and 2 patients with ^{18}F-FDG–negative aneurysms. Four patients had a follow-up PET/CT to reevaluate their cancer. The vascular calcification and ^{18}F-FDG findings were essentially unchanged.

Carotid arteries displayed ^{18}F-FDG accumulation more often than arterial calcification (31% vs. 19%). ^{18}F-FDG uptake was often unilateral (61%) and focal. Calcification was often bilateral (62%). No correlation was found between the presence of cardiovascular risk factors and either carotid ^{18}F-FDG uptake ($P = 1.0$) or calcification ($P = 0.1$). Of 6 patients with prior carotid endarterectomies, 4 displayed ipsilateral increased carotid ^{18}F-FDG uptake. Five of 6 surgeries were performed >12 mo before PET.

TABLE 2
Prevalence of ^{18}F-FDG Uptake or Calcification in Major Arteries

Artery	^{18}F-FDG only	Calcium only	Neither	Both
Right iliac	2 (2)	31 (39)	25 (31)	22 (28)
Left iliac	4 (5)	27 (34)	28 (35)	21 (26)
Aorta	9 (11)	7 (8)	16 (20)	50 (60)
Abdominal	7 (8)	20 (24)	22 (28)	33 (40)
Desc thoracic	14 (18)	21 (26)	32 (41)	12 (15)
Proximal	20 (25)	15 (19)	21 (27)	23 (29)
Right carotid	13 (17)	8 (10)	50 (65)	6 (8)
Left carotid	15 (19)	5 (7)	50 (65)	7 (9)
Any coronary	5 (7)	33 (48)	14 (20)	17 (25)
Left main	10 (21)	9 (19)	26 (56)	2 (4)
Left anterior desc	3 (6)	16 (34)	24 (51)	4 (9)
Circumflex	4 (9)	9 (19)	28 (59)	6 (13)
Right	2 (4)	13 (28)	30 (64)	2 (4)
Posterior desc	2 (4)	3 (6)	42 (90)	0 (0)

Desc = descending.
Seventy-eight patients had 82 studies. Number of studies and percentages of studies (in parentheses) are listed. Peripheral and coronary arteries of some patients were excluded from analysis.

Two patients suffered cerebrovascular accidents, 2 and 39 d after PET/CT, respectively. PET/CT studies of both patients showed ^{18}F-FDG accumulation in the carotid artery perfusing the territory of the cerebrovascular accident (Fig. 4).

Thirty-four patients with intense myocardial uptake were excluded from analysis of coronary activity. ^{18}F-FDG was detected most often in the first centimeter-segments of the left main coronary artery (26%), left circumflex artery (LCX) (21%), left anterior descending artery (LAD) (15%), right coronary artery (RCA) (9%), and posterior descending artery (PDA) (4%), involving >1 coronary territory in 47% of cases (Fig. 5). Differences in prevalence were insignificant ($P = 0.1$). Hepatic ^{18}F-FDG often obscured evaluation of the diaphragmatic aspect of the heart. Coronary calcification was identified in the LAD (42%), followed by LCX (32%), RCA (32%), left main coronary artery (LMA) (23%), and PDA (6%).

Thirty-two patients had MPI studies available for correlation. The median interval between PET and MPI studies was 31 d. Sixteen MPI studies were reported as abnormal, including 8 that showed evidence of ischemia. Eight patients with abnormal MPI had myocardial ^{18}F-FDG uptake and were excluded from analysis. The Fisher exact test found a significant correlation ($P < 0.03$) between abnormal MPI and coronary ^{18}F-FDG uptake. Of the 5 cases with both abnormal MPI and coronary ^{18}F-FDG uptake, the same (i.e., concordant) coronary territories were involved in 2 of the pairs of studies.

No cardiac events occurred during follow-up (average, 7 mo). The prevalence of coronary ^{18}F-FDG increased as the number of cardiac risk factors increased (Table 4). Patients with a history of CAD ($n = 19$) had 4-fold greater odds of coronary ^{18}F-FDG (OR, 4.1; 95% CI, 1.0, 16.2; $P = 0.05$).

TABLE 3
Odds of ^{18}F-FDG Uptake Depending on Calcification in Major Arteries

Artery	OR	95% CI	P value*
Aorta			
Abdominal	5.1	(1.8, 4.3)	0.001
Desc thoracic	1.3	(0.5, 3.3)	0.6
Proximal	1.6	(0.6, 3.9)	0.37
Right carotid	2.8	(0.8, 9.8)	0.09
Left carotid	4.7	(1.3, 16.8)	0.03
Any coronary	3.7	(1.0, 13.2)	0.07
Left main	0.6	(0.1, 3.1)	0.70
Left anterior desc	2.0	(0.4, 10.1)	0.43
Circumflex	4.7	(1.1, 20.3)	0.05
Right	2.3	(0.3, 18.2)	0.58

*$P = 0.005$ is considered significant.
Desc = descending; OR = odds ratio; CI = confidence interval.
Peripheral and coronary arteries of some patients were excluded from analysis.

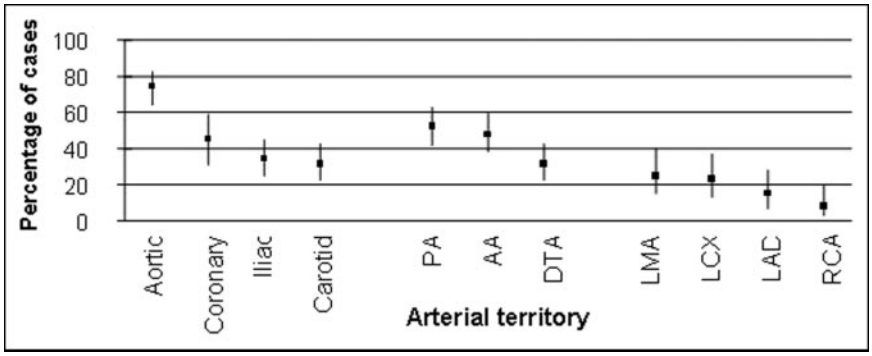

FIGURE 2. Plot illustrates distribution of ^{18}F-FDG, in arterial tree, as percentage of cases; 95% confidence intervals are shown. PA = proximal aorta; AA = abdominal aorta; DTA = descending thoracic aorta; LMA = left main coronary artery; LCX = circumflex coronary artery; LAD = left anterior descending coronary artery; RCA = right coronary artery.

Four of 8 post–coronary artery bypass graft patients demonstrated coronary ^{18}F-FDG.

DISCUSSION

Atherosclerosis is an immune inflammatory disease (*17*) with various postulated triggers (*1*). Macrophage-secreted metalloproteinases contribute to the medial atrophy of AAA (*18*) and concentrate in the intimomedial junctions of coronary plaques during positive remodeling (*19*), with an associated vulnerability to rupture (*20*).

Calcium deposits in the vasculature, especially in the coronary arteries, are pathognomonic of atherosclerosis (*21,22*). Although calcification is often considered the end stage of atheroma, it may be found in earlier stages (*3*). Monocytes, intralesional macrophages, vesicles from apoptotic cells, and the death of vascular smooth muscle cells have been implicated in vascular calcification (*23–25*).

FDG Imaging

The ability of PET to visualize ^{18}F-FDG uptake by atheroma has been validated by several histopathologic studies, including a recent experimental study by Ogawa et al. (*6*).

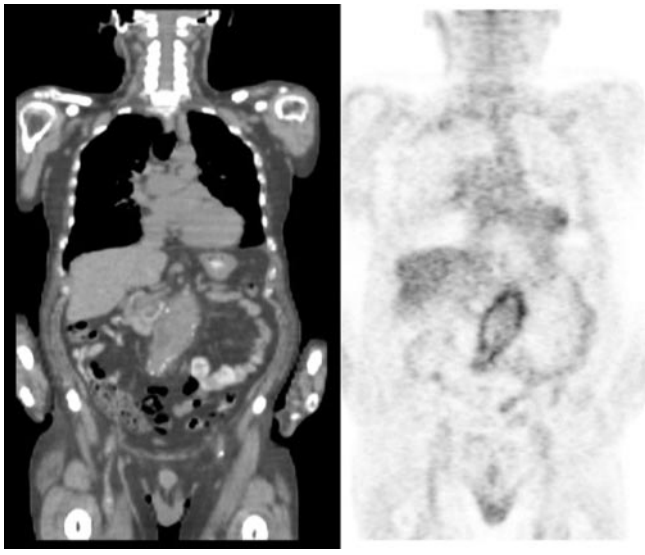

FIGURE 3. Coronal CT (left) and PET (right) images show intense mural inflammation in AAA.

^{18}F-FDG concentrates in inflammatory cells (*7*), allowing imaging of inflammation by PET (*26*). Immune cell activation is associated with increased oxidative metabolism, which is reflected by an increased rate of glucose use (*27*).

Several factors can alter ^{18}F-FDG distribution. Principal among these is hyperglycemia. Blood sugars measured at the time of ^{18}F-FDG injection revealed euglycemia in our patients. In addition, some forms of therapy, such as steroids, may reduce the level of uptake in the vasculature. Three patients in our series were on potent antiinflammatory drugs, one each on dexamethasone, prednisone, and tacrolimus. Each had significant vascular ^{18}F-FDG uptake.

Arterial ^{18}F-FDG accumulation was consistent with atherosclerotic topography (*28,29*). ^{18}F-FDG uptake was most prevalent in the aorta, followed by the coronary and carotid arteries ($P < 0.0001$). In the aorta, ^{18}F-FDG uptake was most prevalent in the proximal segment ($P = 0.01$), which is the earliest site for atherosclerosis (*28*). Tatsumi et al. (*12*) found ^{18}F-FDG uptake in 59% of thoracic aortae, whereas we found uptake in 77%. Abdominal aortic ^{18}F-FDG uptake was more diffuse and more prevalent (56%) than uptake in the descending thoracic aorta, where a posterior predilection was observed (*28*). Meller et al. (*30*) found no ^{18}F-FDG uptake in the abdominal aorta. Yun et al. (*11*) found ^{18}F-FDG uptake in 53% of abdominal aortae. The different findings may reflect the contribution of CT fusion in localizing arterial ^{18}F-FDG accumulation.

Territorial calcification and ^{18}F-FDG uptake were associated (Table 3), yet rarely overlapped, in our study. A recent study by Ben-Haim et al. (*31*) used PET/CT to determine the relationship between arterial ^{18}F-FDG and calcification. On a lesion-by-lesion basis, they found both calcium and ^{18}F-FDG present in 10% of lesions, which is a higher fraction of patients than we observed. However, our methodology corrected for residual circulating ^{18}F-FDG, which may reduce the ability to identify lesions with low levels of ^{18}F-FDG uptake. As observed in the Ben-Haim study, we found no difference in vascular ^{18}F-FDG uptake, at calcified sites, on uncorrected images.

AAA

AAA are characterized by transmural inflammation, with lymphocyte and macrophage aggregation (*32*). Our data

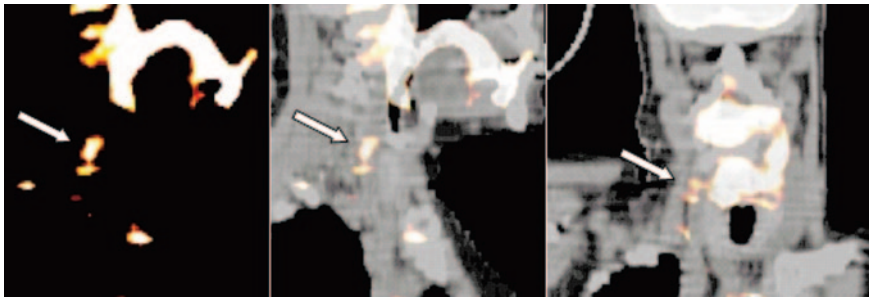

FIGURE 4. (Left to right) PET and PET/CT images show foci of inflammation in right common carotid artery (arrows), from lateral (left) and right oblique (right) projections. Two days later, patient suffered a right-sided cerebrovascular accident.

hinted at a possible correlation between AAA size and ^{18}F-FDG uptake, but our sample size was small (n = 6). Sakalihasaan et al. (*33*) reported that AAA patients with negative PET (16/26) required no urgent aneurysmal surgery, whereas 6 patients with ^{18}F-FDG–avid AAA required vascular surgery within a short period.

Coronary Arteries

Coronary ^{18}F-FDG uptake was most often proximal (*34*) and multifocal, which agrees with autopsy studies that coronary inflammation occurs at multiple sites simultaneously (*35*). Patients with coronary ^{18}F-FDG uptake were 4 times more likely to have documented CAD, but larger studies are needed to verify this finding.

The current 4- to 5-mm spatial resolution of PET contributes to the challenge of identifying coronary activity. Yet atherosclerotic inflammation can involve the intima, adventitia, and even underlying myocardium (*36*), theoretically increasing the signal region of ^{18}F-FDG uptake. With sufficient ^{18}F-FDG accumulation, size becomes less relevant in lesion detection.

The combination of limited PET spatial resolution and cardiac motion reduces the sensitivity of PET in the coronary arteries. Coronary motion is greatest in the RCA, followed in descending order by the circumflex artery, LAD, and LMA (*37*). Motion artifact, therefore, would be expected to reduce the sensitivity of PET for coronary ^{18}F-FDG activity in that order. Our study found a lower incidence of ^{18}F-FDG in the RCA compared with the LMA.

Subsequent studies might explore enhancing visualization of coronary ^{18}F-FDG accumulation by a combination of gating to reduce motion and pharmacologic methods (*38*) to either increase ^{18}F-FDG uptake in atherosclerotic coronary lesions or decrease background in normal myocardium (*39*).

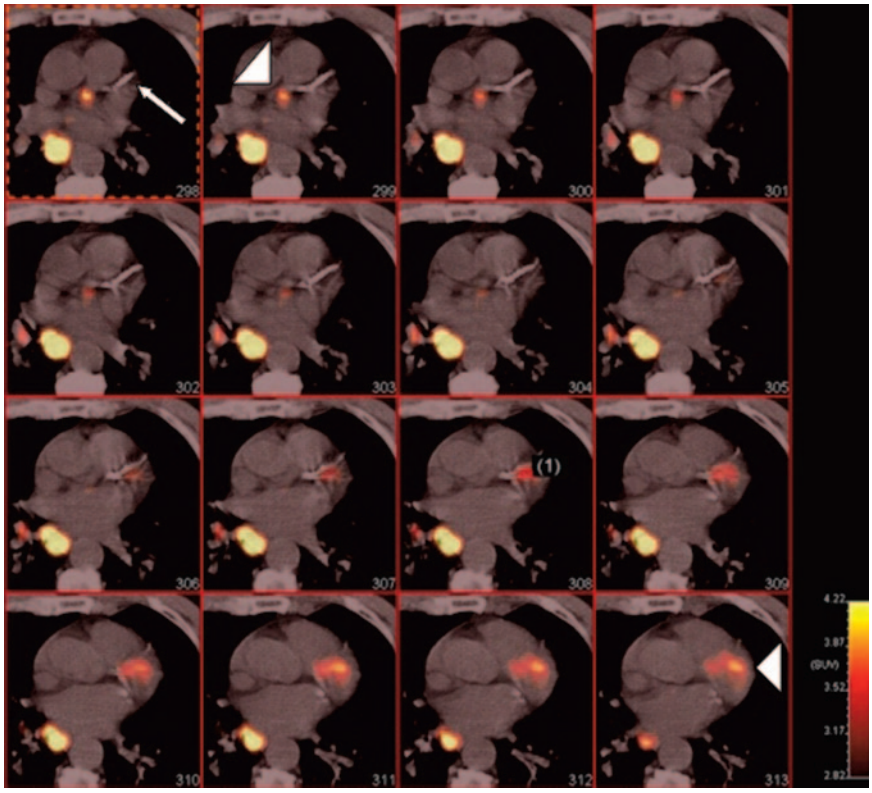

FIGURE 5. Fused PET/CT images show contiguous transaxial slices through heart. Inflammation (arrowheads) present proximal and distal to a calcified LAD (arrow). A tumor sits adjacent to esophagus.

TABLE 4
Clinical Characteristics of Patients Displaying Coronary ^{18}F-FDG Uptake (n = 22)

Patient no.	CA*	Age (y)	Sex	Prior angioplasty	Prior CABG	ASVD	HTN	DM	High chol	Smoking	Abnormal MPI†
1	G	81	M	Y	Y	Y	Y	N	Y	N	N (+28)
2	GI	78	M	N	N	N	N	N	N	N	Y (−1)
3	GI	79	M	N	N	Y	N	N	Y	Y	N (+1)
4	GI	64	F	N	N	N	Y	N	Y	N	Y (+56)
5	R	61	F	N	N	N	N	N	N	Y	NA
6	GI	76	F	Y	Y	Y	Y	N	N	Y	N (+11)
7	N	72	F	Y	Y	Y	Y	N	Y	N	Y (+365)
8	R	78	M	Y	N	Y	Y	N	N	Y	Y (+59)
9	H	67	M	N	N	Y	Y	N	Y	Y	NA
10	R	56	M	N	N	N	N	Y	Y	N	NA
11	H	70	M	N	N	N	N	N	Y	Y	NA
12	E	55	F	Y	N	Y	N	Y	Y	Y	NA
13	GI	77	M	N	N	Y	Y	Y	N	Y	Y (−219)
14	H	75	M	N	Y	Y	N	N	Y	Y	NA
15	H	45	F	N	N	N	N	N	N	N	N (+350)
16	E	74	F	N	N	N	Y	N	N	N	NA
17	GI	83	M	N	N	N	N	N	N	N	NA
18	R	71	M	Y	N	Y	Y	N	Y	N	NA
19	N	71	M	N	Y	Y	N	N	N	N	Y (−3)
20	GI	58	M	N	N	N	N	N	N	N	NA
21	GI	63	M	N	N	Y	Y	N	Y	Y	Y (−156)
22	E	66	M	N	N	N	N	N	N	N	NA

*Patients with >1 cancer type were grouped according to most aggressive cancer. G = genitourinary; GI = gastrointestinal; R = respiratory tract; N = no cancer; H = hematologic; E = endocrine.

†Days before (−) or after (+) PET in parentheses. NA = MPI data unavailable.

ASVD = atherosclerotic vascular disease; HTN = hypertension; DM = diabetes; High chol = hypercholesterolemia; Smoking = history of smoking; MPI = MPI findings.

For each variable, patients without documented history or with documentation of not having a condition are both listed as N. Y indicates documented history.

Critique of Methodology and Limitations

By raising the lower threshold of the PET color scale, we probably suppressed some vascular ^{18}F-FDG accumulation. Identification of vascular lesions may be enhanced, if, as suggested by Rudd et al. (*10*), the interval between injection and imaging was increased beyond the standard 1-h postinjection delay to improve target-to-background ratios. This is also suggested by in vitro studies, where macrophages accumulate ^{18}F-FDG without a plateau for at least 3 h (*27*).

We could not evaluate coronary uptake in about half of our patients because of intense myocardial uptake. This high frequency of myocardial uptake is similar to the results of Ding et al. (*40*). Preliminary studies in animals suggest that native myocardial ^{18}F-FDG uptake can be reduced by β-blockade (*39*). Coronary vessels move 7–23 mm during the cardiac cycle (*16*), and coronary ^{18}F-FDG visualization likely would be improved by electrocardiographic gating.

CONCLUSION

This study suggests that vascular inflammation, as defined by ^{18}F-FDG uptake, and vascular calcification identify different phases of atherosclerosis. Although both ^{18}F-FDG uptake and calcification often occur in the same vessel, they rarely occur at the same site within the vessel. Combined anatomic and metabolic imaging with ^{18}F-FDG PET/CT offers promise as a noninvasive method of indicating atheromas, because the combination of technologies appears to identify plaque at different phases of the lesion.

REFERENCES

1. Libby P. Inflammation in atherosclerosis. *Nature.* 2002;420:868–874.
2. MacNeill BD, Jang IK, Bouma BE, et al. Focal and multi-focal plaque macrophage distributions in patients with acute and stable presentations of coronary artery disease. *J Am Coll Cardiol.* 2004;44:972–979.
3. Trion A, van der Laarse A. Vascular smooth muscle cells and calcification in atherosclerosis. *Am Heart J.* 2004;147:808–814.
4. Vallabhajosula S, Machac J, Knesaurek K, et al. Imaging atherosclerotic macrophage density by positron emission tomography using F-18 fluorodeoxyglucose (FDG) [abstract]. *J Nucl Med.* 1996;37(suppl):38P.
5. Tokita N, Zanzonico P, Dunphy M, et al. FDG-PET detected infiltration of inflammatory cells around coronary arteries as a marker for atherosclerosis [abstract]. *Eur J Nucl Med Mol Imaging*. 2004;31(suppl 2):S203.
6. Ogawa M, Ishino S, Mukai T, et al. ^{18}F-FDG accumulation in atherosclerotic plaques: immunohistochemical and PET imaging study. *J Nucl Med.* 2004;45:1245–1250.
7. Kaim AH, Weber B, Kurrer MO, et al. Autoradiographic quantification of

[18]F-FDG uptake in experimental soft-tissue abscesses in rats. *Radiology.* 2002; 223:446–451.
8. Kubota R, Kubota K, Yamada S, Tada M, Ido T, Tamahashi N. Microautoradiographic study for the differentiation of intratumoral macrophages, granulation tissues and cancer cells by the dynamics of fluorine-18-fluorodeoxyglucose uptake. *J Nucl Med.* 1994;35:104–112.
9. Vallabhajosula S, Fuster V. Atherosclerosis: imaging techniques and the evolving role of nuclear medicine. *J Nucl Med.* 1997;38:1788–1796.
10. Rudd JHF, Warburton EA, Fryer TD, et al. Imaging atherosclerotic plaque inflammation with [18]F-fluorodeoxyglucose positron emission tomography. *Circulation.* 2002;105:2708–2711.
11. Yun M, Jang S, Cucchiara A, Newberg AB, Alavi A. [18]F FDG uptake in the large arteries: a correlation study with the atherogenic risk factors. *Semin Nucl Med.* 2002;32:70–76.
12. Tatsumi M, Cohade C, Nakamoto Y, Wahl RL. Fluorodeoxyglucose uptake in the aortic wall at PET/CT: possible finding for active atherosclerosis. *Radiology.* 2003;229:831–837.
13. Doherty TM, Asotra K, Fitzpatrick LA, et al. Calcification in atherosclerosis: bone biology and chronic inflammation at the arterial crossroads. *Proc Natl Acad Sci USA.* 2003;100:11201–11206.
14. Sangiorgi G, Rumberger JA, Severson A, et al. Arterial calcification and not lumen stenosis is highly correlated with atherosclerotic plaque burden in humans: a histologic study of 723 coronary artery segments using non-decalcifying methodology. *J Am Coll Cardiol.* 1998;31:126–133.
15. Agatston AS, Janowitz W, Hildner FJ, Zusmer NR, Viamonte M, Detrano R. Quantification of coronary artery calcium using ultrafast computed tomography. *J Am Coll Cardiol.* 1990;15:827–832.
16. Wang Y, Vidan E, Bergman GW. Cardiac motion of coronary arteries: variability in the rest period and implications for coronary MR angiography. *Radiology.* 1999;213:751–758.
17. Schwartz CJ, Valente AJ, Sprague EA, Kelley JL, Suenram CA, Rozek MM. Atherosclerosis as an inflammatory process: the roles of the monocyte-macrophage. *Ann NY Acad Sci.* 1985;454:115–120.
18. Yamashita A, Noma T, Nakazawa A, et al. Enhanced expression of matrix metalloproteinase-9 in abdominal aortic aneurysms. *World J Surg.* 2001;25:259–265.
19. Pasterkamp G, Schoneveld AH, Hijnen DJ, et al. Atherosclerotic arterial remodeling and the localization of macrophages and matrix metalloproteases 1, 2 and 9 in the human coronary artery. *Atherosclerosis.* 2000;150:245–253.
20. Burke AP, Kolodgie FD, Farb A, Weber D, Virmani R. Morphological predictors of arterial remodeling in coronary atherosclerosis. *Circulation.* 2002;105:297–303.
21. Rumberger JA, Simons DB, Fitzpatrick LA, Sheedy PF, Schwartz RS. Coronary artery calcium area by electron-beam computed tomography and coronary atherosclerotic plaque area: a histopathologic correlative study. *Circulation.* 1995; 92:2157–2162.
22. Becker CR, Kleffel T, Crispin A, et al. Coronary artery calcium measurement: agreement of multirow detector and electron beam CT. *AJR.* 2001;176:1295–1298.
23. Jeziorska M, McCollum C, Woolley DE. Calcification in atherosclerotic plaque of human carotid arteries: associations with mast cells and macrophages. *J Pathol.* 1998;185:10–17.
24. Tintut Y, Patel P, Territo M, Saini T, Parhami F, Demer LL. Monocyte/macrophage regulation of vascular calcification in vitro. *Circulation.* 2002;105:650–655.
25. Mohler ER, Gannon G, Reynolds C, Zimmerman R, Keane MG, Kaplan FS. Bone formation and inflammation in cardiac valves. *Circulation.* 2001;103:1522–1528.
26. Osman S, Danpure HJ. The use of 2-[[18]F]fluoro-2-deoxy-D-glucose as a potential in vitro agent for labelling human granulocytes for clinical studies by positron emission tomography. *Int J Rad Appl Instrum B.* 1992;19:183–190.
27. Deichen JT, Prante1 O, Gack1 M, Schmiedehausen K, Kuwert T. Uptake of [[18]F]fluorodeoxyglucose in human monocyte-macrophages in vitro. *Eur J Nucl Med Mol Imaging.* 2003;30:267–273.
28. Holman RL, McGill HC, Strong JP, Geer JC. The natural history of atherosclerosis: the early aortic lesions as seen in New Orleans in the middle of the 20th Century. *Am J Pathol.* 1958;34:209–235.
29. McGill HC Jr, Arias-Stella J, Carbonell LM, et al. General findings of the International Atherosclerosis Project. *Lab Invest.* 1968;18:38–42.
30. Meller J, Strutz S, Siefker U, et al. Early diagnosis and follow-up of aortitis with [[18]F]FDG PET and MRI. *Eur J Nucl Med Mol Imaging.* 2003;30:730–736.
31. Ben-Haim S, Kupzov E, Tamir A, Israel O. Evaluation of [18]F-FDG uptake and arterial wall calcifications using [18]F-FDG PET/CT. *J Nucl Med.* 2004;45:1816–1821.
32. Ailawadi G, Eliason JL, Upchurch GR. Current concepts in the pathogenesis of abdominal aortic aneurysm. *J Vasc Surg.* 2003;38:584–588.
33. Sakalihasan N, Van Damme H, Gomez P. Positron emission tomography (PET) evaluation of abdominal aortic aneurysm (AAA). *Eur J Vasc Endovasc Surg.* 2002;23:431–436.
34. Montenegro MR, Eggen DA. Topography of atherosclerosis in the coronary arteries. *Lab Invest.* 1968;18:126–133.
35. Spagnoli LG, Bonanno E, Mauriello A. Multicentric inflammation in epicardial coronary arteries of patients dying of acute myocardial infarction. *J Am Coll Cardiol.* 2002;40:1579–1588.
36. Laine P, Kaartinen M, Penttila A, Panula P, Paavonen T, Kovanen PT. Association between myocardial infarction and the mast cells in the adventitia of the infarct-related coronary artery. *Circulation.* 1999;99:361–369.
37. Lu B, Mao SS, Zhuang N, et al. Coronary artery motion during the cardiac cycle and optimal ECG triggering for coronary artery imaging. *Invest Radiol.* 2001; 36:250–256.
38. Frostegard J, Ulfgren AK, Nyberg P. Cytokine expression in advanced human atherosclerotic plaques: dominance of pro-inflammatory (Th1) and macrophage-stimulating cytokines. *Atherosclerosis.* 1999;145:33–43.
39. Tokita N, Zanzonico P, Dunphy M, et al. Suppression of physiological myocardial fluorodeoxyglucose uptake [abstract]. *J Am Coll Cardiol.* 2004;43(suppl A):337A.
40. Ding HJ, Shiau YC, Wang JJ, Ho ST, Kao A. The influences of blood glucose and duration of fasting on myocardial glucose uptake of [[18]F]fluoro-2-deoxy-D-glucose. *Nucl Med Commun.* 2002;23:961–965.

JNM The Journal of NUCLEAR MEDICINE

Association of Vascular ^{18}F-FDG Uptake with Vascular Calcification

Mark P.S. Dunphy, Alvin Freiman, Steven M. Larson and H. William Strauss

J Nucl Med. 2005;46:1278-1284.

The Journal of Nuclear Medicine is published monthly.
SNMMI | Society of Nuclear Medicine and Molecular Imaging
1850 Samuel Morse Drive, Reston, VA 20190.
(Print ISSN: 0161-5505, Online ISSN: 2159-662X)

SNMMI SOCIETY OF NUCLEAR MEDICINE AND MOLECULAR IMAGING